

Chapter 1

Extinction and Recovery of Superconductivity by Interference in Superconductor/Ferromagnet Bilayers

A.S. Sidorenko, V.I. Zdravkov, J. Kehrle, R. Morari, E. Antropov,
G. Obermeier, S. Gsell, M. Schreck, C. Müller, V.V. Ryazanov, S. Horn,
R. Tidecks, and L.R. Tagirov

Abstract In superconductor–ferromagnet (S/F) metallic contacts, the superconducting condensate penetrates through the S/F interface into a ferromagnetic layer. In contrast to the conventional S/N proximity effect, the pairing wave function not only decays deep into the F metal, but simultaneously oscillates. Interference of the oscillating pairing function in a ferromagnetic film gives rise to a modulation of the pairing function flux crossing the S/F interface, which results in oscillations of superconducting transition temperature of the adjacent S layer. In this work, we report on the experimental observation of the superconductivity reentrance phenomenon with double suppression of the superconductivity in Nb/Cu_{1-x}Ni_x bilayers as a function of the ferromagnetic layer thickness, d_{CuNi} . The superconducting T_c drops sharply with increasing d_{CuNi} till total suppression of superconductivity at $d_{\text{CuNi}} \approx 2.5$ nm. At a further increase of the Nb/Cu_{1-x}Ni_x layer thickness, the superconductivity restores at $d_{\text{CuNi}} \geq 24$ nm. Then, with the subsequent increase of d_{CuNi} , the superconductivity vanishes again at $d_{\text{CuNi}} \approx 38$ nm.

1.1 Introduction

In superconductor–ferromagnetic metal (S/F) contacts, the superconducting pairing wave function not only exponentially decays into the F metal, as in the superconductor/normal metal (S/N) proximity effect [1, 2], but simultaneously oscillates [3, 4]. A variety of novel physical effects caused by these oscillations was predicted (see reviews [5–8] and references therein). Some of them have already been observed experimentally: nonmonotonous behavior of the superconducting critical temperature, T_c , as a function of the F metal layer thickness [9–13], Josephson junctions with intrinsic π -phase shift across the junction [14], and inverted, cap-sized differential current–voltage characteristics [15]. In this work, we report on results of observation of the reentrant T_c phenomenon with double suppression of superconductivity in Nb/Cu_{1-x}Ni_x bilayers ($x = 0.59$) for increasing ferromagnetic Cu_{1-x}Ni_x layer thickness, d_{CuNi} . After a destruction by interference effects of the superconducting pairing wave function and a subsequent recovery, a second suppression of

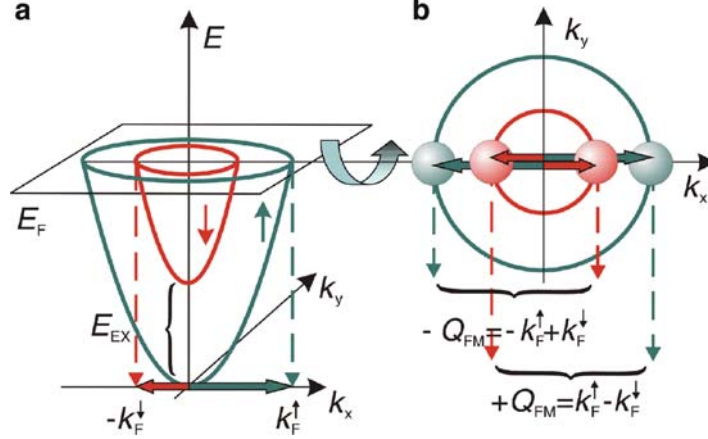


Fig. 1.1 Origin of the FFLO state. (a) Spin-splitting E_{ex} of the conduction band of a ferromagnet by the exchange field. Sketch for $k_z = 0$. (b) Cross-section of the band energy dispersions for $k_z = 0$ at the Fermi energy. Paired electrons (green with red balls) establish from the majority (green) and minority (red) subbands (wave number vectors indicated in the respective color). The FFLO pairing momentum along the x axis is $\hbar Q_{FM} = \hbar \Delta k_F = E_{ex}/v_F$

superconductivity is found, giving an impressive experimental evidence for a quasi-one dimensional Fulde–Ferrell–Larkin–Ovchinnikov (FFLO) [16, 17] like state in the ferromagnetic layer.

At a plane S/F interface, the quasi-one-dimensional FFLO-like state can be generated in the F material [3–8]. Due to the exchange splitting of the conduction band (Fig. 1.1a), one of the singlet Cooper-pair electrons occupies the majority subband, e.g., spin-up, while the other one resides at the spin-down, minority subband (Fig. 1.1b). Although the pairing occurs with opposite directions of the wave number vectors of the electrons, their absolute values are not equal due to the exchange splitting of the conduction band (see Fig. 1.1a). The resulting pairing state acquires a finite momentum of $\hbar Q_{FM} = E_{ex}/v_F$, where $E_{ex} \ll E_F$ is the energy of the exchange splitting of a free-electron-like, parabolic conduction band, E_F is the Fermi energy, and v_F is the Fermi velocity. Then, the pairing function of this state does not simply decay as it would be in a nonmagnetic metal, but oscillates on a wavelength scale λ_{FM} (i.e., $\lambda_{FM} = 2\pi/k_{FM}$) given by the magnetic coherence length ξ_F . In a clean ferromagnet ($l_F \gg \xi_{F0}$), it is $\lambda_{F0} \equiv 2\pi\xi_{F0} = 2\pi\hbar v_F/E_{ex}$ [4, 18], whereas in the dirty case ($l_F \ll \xi_{F0}$), we get $\lambda_{FD} = 2\pi\xi_{FD} = 2\pi (2\hbar D_F/E_{ex})^{1/2}$ [3, 7], where $D_F = l_F v_F/3$ with l_F the electron mean free path in the F-metal. The decay length of the pairing wave function is l_F and ξ_{FD} in the clean and dirty cases respectively [3, 4, 19].

The oscillation of the pairing wave function in the F-metal is the reason for an oscillatory S/F proximity effect, yielding a nonmonotonous, oscillating dependence of the superconducting critical temperature, T_c , on the ferromagnetic layer thickness, d_F . The phenomenon can be qualitatively described using the analogy

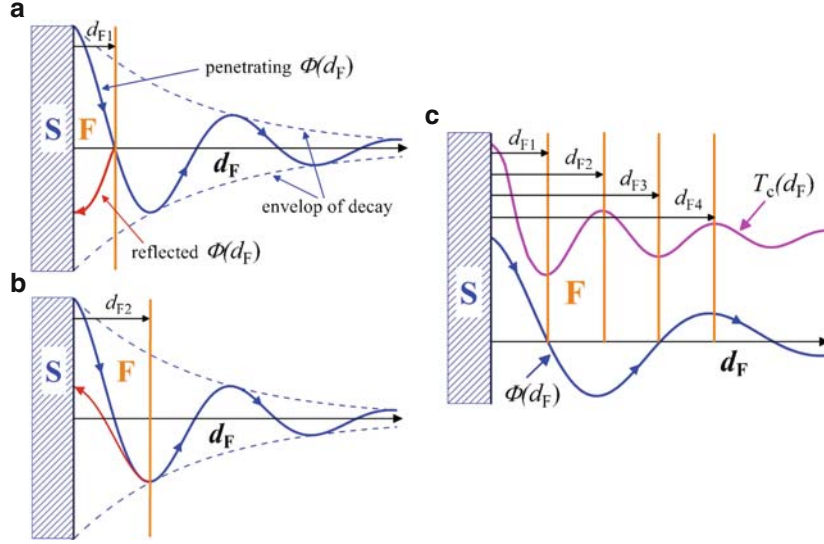


Fig. 1.2 Interference of the pairing function Φ in an S/F bilayer at the S/F interface assuming the case that $1/2$ of the pairing function amplitude is reflected at the boundary, and $1/2$ penetrates into the F material. Spin-dependent phase-shifts of the penetrating pairing function at the S/F interface [21–23] as well as phase shifts for the reflected waves are neglected for simplicity. (a) For $d_{F1} \sim \lambda_{FM}/4$ the resulting amplitude is minimal. (b) For $d_{F2} \sim \lambda_{FM}/2$ the subsequent local maximum of the amplitude is reached for increasing d_F . (c) Modulation of the superconducting transition temperature T_c of a thin superconducting film correlated with the interference conditions

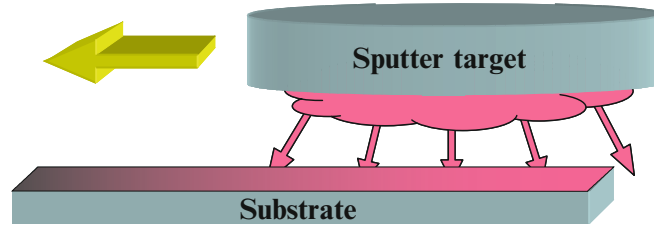


Fig. 1.3 The moving target setup utilizing the spray deposition technique

with the interference of light in a parallel-sided plate of glass with a mirror coated back side, at normal incidence [20]. As the interference conditions change periodically between constructive and destructive upon changing the thickness of the plate, the flux of light through the interface of incidence is modulated. In a layered S/F system, the pairing function flux crossing the S/F interface depends on the ferromagnetic layer thickness, d_F , because of the pairing function interference (see Fig. 1.2a, b). As a result, the coupling between the S and F layers in a series of samples with increasing d_F is modulated, and the superconducting T_c oscillates as a function of d_F (Fig. 1.2c). The amplitude of T_c oscillation depends sensitively on the superconducting layer thickness (see discussion of Fig. 1.3a, b).

Recently, expressed oscillations and pronounced reentrance, i.e., an extinction and recovery of superconductivity as a function of d_F , were measured in a Nb/Cu_{1-x}Ni_x bilayer [13]. However, the most spectacular evidence for the oscillatory proximity effect would be the observation of the multiple reentrant behavior of the superconducting state predicted theoretically [19, 24, 25]. To realize this regime experimentally, one has to study at first the $T_c(d_S)$ dependence for a series of S/F bilayers with constant d_F to find the range of the superconducting layer thickness, d_S , in which superconductivity is most sensitive to the destructive influence of the ferromagnetism.

1.2 Sample Preparation and Characterization

To fabricate the S/F bilayers, we used niobium as superconducting material and Cu_{1-x}Ni_x ($x \approx 0.59$) alloy as ferromagnetic layer. The choice of the alloy instead of a conventional elemental ferromagnet has the following advantages for the experimentalist. The oscillation length $\lambda_{F0} = 2\pi\hbar v_F/E_{ex}$ in strong clean ferromagnets, like iron, nickel, or cobalt, is extremely short, because the exchange splitting energy, E_{ex} , is usually in the range 0.1–1.0 eV [9, 10, 12, 26]. Thus, to detect an oscillatory behavior of T_c experimentally, d_F must be very small, e.g., between 0.6 and 2.5 nm for pure Ni [26]. Weak ferromagnets with an order of magnitude smaller exchange splitting of the conduction band allow the observation of the effect at much larger thicknesses d_F of about 2–25 nm, which can be controlled and characterized more easily. Moreover, for a long-wavelength oscillation, the atomic-scale interface roughness does not any longer have a dominating effect on an extinction of T_c oscillations.

The S/F samples were prepared by magnetron sputtering on commercial (111) silicon substrates at room temperature. Three targets, Si, Nb, and Cu₄₀Ni₆₀ (75 mm in diameter), were presputtered for 10–15 min to remove contaminations and reduce the residual gas pressure (by Nb as getter material) in the chamber. First, a silicon buffer layer was deposited using a RF magnetron to generate a clean interface for the subsequently deposited Cu_{1-x}Ni_x or niobium layer.

To prepare samples with variable thickness of one of the layers, a wedge-shaped film was deposited [13, 26]: the 80 mm long and 7 mm wide silicon substrate was mounted at a distance of 4.5 cm from the target symmetry axis to utilize the intrinsic spatial gradient of the deposition rate. The Cu₄₀Ni₆₀ target was RF sputtered with a rate 3–4 nm sec⁻¹.

To obtain flat, high-quality Nb layers with thicknesses in the range of 5–15 nm, we moved the full-power operating magnetron along the silicone substrate using the motorized setup (see Fig. 1.3). Thus, the surface was uniformly sprayed with the material, and the average deposition rate of the Nb film could be decreased down to 1.3 nm sec⁻¹, while for a fixed, nonmoving target, it would be about 4 nm sec⁻¹. To prevent degradation in an ambient atmosphere, the resulting Cu_{1-x}Ni_x/Nb or Nb/Cu_{1-x}Ni_x bilayers were coated by an amorphous silicon cap of about 10 nm

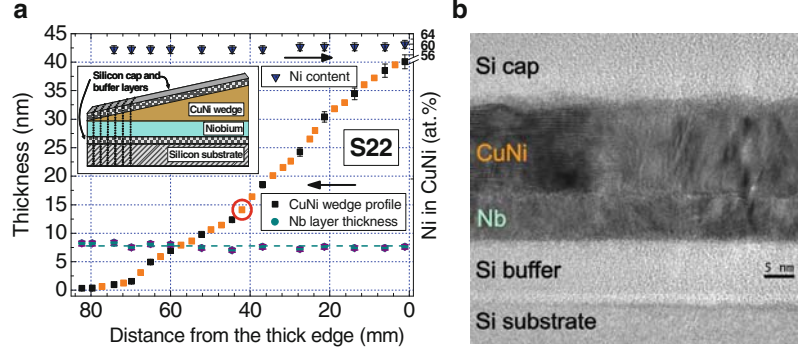


Fig. 1.4 Sample design and characterization. **(a)** RBS results for the thickness of the Nb and CuNi layers and Ni content in the CuNi alloy. Sketch of the layers stack, see the inset. Black rectangular symbols for CuNi alloy layer are measured points, orange symbols were linearly interpolated. **(b)** Transmission electron microscopy (TEM) cross-sectional image of a cut across the layers (sample S22-18 marked by a red circle in the left panel: $d_{\text{Nb}} \approx 7.8$ nm, $d_{\text{CuNi}} \approx 14$ nm according to RBS)

thickness, which is insulating at low temperatures. After cutting the wedge samples into strips across the thickness gradient (see the inset in Fig. 1.4a), aluminum wires 50 μm in diameter were attached to the strips by an ultrasonic bonder for four-probe resistance measurements. For further sample preparation details, see [13, 26].

In the first kind of samples, the superconducting Nb layer was of variable thickness, $d_{\text{Nb}} \approx 4\text{--}47$ nm, prepared utilizing the wedge deposition technique described earlier. The $\text{Cu}_{1-x}\text{Ni}_x$ layer was flat with a thickness fixed at a physically infinite value of $d_{\text{CuNi}} = 56$ nm [13].

In the second kind of samples, the superconducting Nb layer was flat with a thickness fixed at a selected value in the range 6–15 nm. The deposition technique with moving magnetron described earlier provided high-quality niobium layers with superconducting T_{c0} of the stand-alone film as high as 5.5 K at $d_{\text{Nb}} \approx 5.7$ nm only. The ferromagnetic layer was wedge-shaped. A sketch of the layers stack is presented in the inset of Fig. 1.4a, and a transmission electron microscopy image of one of the samples is given in Fig. 1.4b. After cutting the final stack into strips across the $\text{Cu}_{1-x}\text{Ni}_x$ wedge gradient, a series of 36–40 samples were obtained with variable $\text{Cu}_{1-x}\text{Ni}_x$ layer thicknesses in the range $d_{\text{CuNi}} \approx 1\text{--}35$ nm, prepared at identical conditions in a single deposition run.

Rutherford backscattering spectrometry (RBS) has been used to evaluate the thickness of Nb and $\text{Cu}_{1-x}\text{Ni}_x$ layers as well as to check the composition of Cu and Ni in the deposited alloy layers (Fig. 1.4a). For details, see [13]. An advantage of RBS is that it is an absolute method that does not require standards for quantification. It allows to determine the thickness (via the areal density) of the layers with an accuracy of $\pm 3\%$ for $\text{Cu}_{1-x}\text{Ni}_x$ on the thick side of the $\text{Cu}_{1-x}\text{Ni}_x$ wedge, and $\pm 5\%$ for Nb and $\text{Cu}_{1-x}\text{Ni}_x$ on the thin side of the wedge. The Ni concentration in the $\text{Cu}_{1-x}\text{Ni}_x$ layer appeared to be almost constant ($x \approx 0.59$), showing a slight increase toward the thick side of the wedge. The thickness of the Nb layer is nearly

constant along the uncut sample, $d_{\text{Nb}} \approx 7.8$ nm. Several samples were studied by TEM, a representative example is given in Fig. 1.4b.

The resistance measurements were performed by the DC four-probe method using a $10 \mu\text{A}$ sensing current in the temperature range 0.4–10 K when measuring with an Oxford Instruments “Heliox” ^3He cryostat, and a $2 \mu\text{A}$ sensing current in the range 40 mK–1.0 K when measuring in an Oxford Instruments dilution refrigerator “Kelvinox”.

1.3 Results of Superconducting T_c Measurements and Discussion

The superconducting critical temperature, T_c , was determined from the midpoints of resistive transitions curves $R(T)$. The width of transition ($0.1R_N$ – $0.9R_N$ criteria, where R_N is the normal state resistance just above T_c) for most of the investigated samples was below 0.2 K, thus allowing to determine the T_c with a good accuracy.

Figure 1.5a demonstrates the dependence of the superconducting transition temperature on the Nb layer thickness, $T_c(d_{\text{Nb}})$. It yields a critical thickness ($d_{\text{Nb}}^{\text{cr}} \approx 5.8$ nm) of the Nb layer down to which superconductivity survives in a metallic

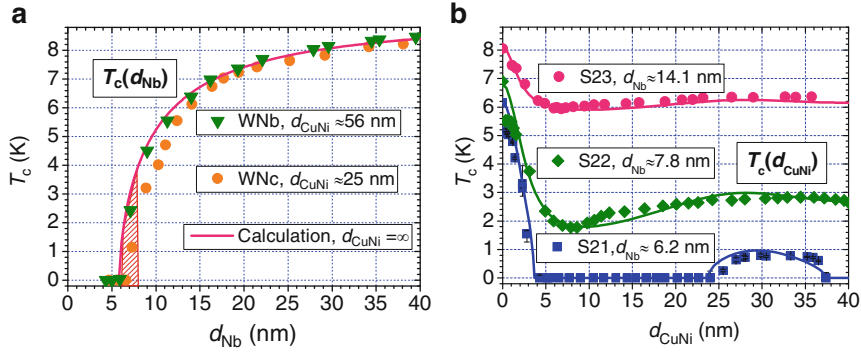


Fig. 1.5 Superconducting T_c as a function of the layer thickness. **(a)** Dependence of the superconducting transition temperature on the niobium layer thickness. Transition widths are within the point size if error bars not visible. The solid line is the result of calculations according to the theory [13, 26] for $d_{\text{CuNi}} \approx 56$ nm, the superconducting coherence length $\xi_S = 11.0$ nm, the ratio of the Sharvin conductances $N_F v_F / N_S v_S = 0.23$, the S/F-interface transparency parameter $T_F = 0.65$, $l_F / \xi_{F0} = 1.1$, $\xi_{F0} = 11.0$ nm. The calculated critical thickness is $d_{\text{Nb}}^{\text{cr}} = 5.8$ nm ($T_c \rightarrow 0$ K). The range of the Nb layer thickness most sensitive to d_{CuNi} variations is shaded in red. **(b)** Non monotonous $T_c(d_F)$ dependence for the Nb/Cu_{1-x}Ni_x bilayers ($x = 0.59$). Solid curves are calculated with values of parameters as follows: (S23) $\xi_S = 10.0$ nm, $N_F v_F / N_S v_S = 0.22$, $T_F = 0.43$, $l_F / \xi_{F0} = 1.1$, $\xi_{F0} = 10.6$ nm; (S22) $\xi_S = 9.8$ nm, $N_F v_F / N_S v_S = 0.22$, $T_F = 0.55$, $l_F / \xi_{F0} = 1.1$, $\xi_{F0} = 10.6$ nm; (S21) $\xi_S = 9.6$ nm, $N_F v_F / N_S v_S = 0.22$, $T_F = 0.59$, $l_F / \xi_{F0} = 1.1$, $\xi_{F0} = 11.0$ nm. The BCS coherence length for Nb was always taken $\xi_{\text{BCS}} = 42$ nm. The calculations give no further reentrance of superconductivity for the S21 sample series above $d_{\text{CuNi}} > 40$ nm

contact with a bulk ferromagnet. The critical thickness is used to determine a constraint on two of the five physical parameters that enter the theory [26]. On the other hand, the $T_c(d_{\text{Nb}})$ measurements provide a range of the Nb layer thickness, within which superconductivity is most sensitive to variations of the magnetic layer thickness (the shaded area indicated in Fig. 1.5a). To observe the reentrant behavior of superconductivity, one should prepare samples with the Nb layer thickness in this range of $d_{\text{Nb}} \approx 6\text{--}8\text{ nm}$.

Figure 1.5b demonstrates the dependence of the superconducting transition temperature on the $\text{Cu}_{41}\text{Ni}_{59}$ layer thickness. The thickness of the flat Nb layer is fixed, $d_{\text{Nb}} \approx 14.1\text{ nm}$ (S23 series), $d_{\text{Nb}} \approx 7.8\text{ nm}$ (S22 series), and $d_{\text{Nb}} \approx 6.2\text{ nm}$ (S21 series). The transition temperature, T_c , for the specimens with $d_{\text{Nb}} \approx 14.1\text{ nm}$ reveals a nonmonotonous behavior with a shallow minimum at about $d_{\text{CuNi}} \approx 7.0\text{ nm}$. For the thinner niobium layer ($d_{\text{Nb}} \approx 7.8\text{ nm}$), the transition temperature shows a pronounced minimum with subsequent increase of T_c to above 2.5 K. For the thinnest Nb layer ($d_{\text{CuNi}} \approx 6.2\text{ nm}$), the superconducting T_c sharply drops upon increasing the ferromagnetic $\text{Cu}_{41}\text{Ni}_{59}$ layer thickness till a certain thickness $d_{\text{CuNi}} \approx 2.5\text{ nm}$. Then, in the range $d_{\text{CuNi}} \approx 2.5\text{--}24\text{ nm}$, the superconducting transition temperature vanishes (T_c is at least lower than the lowest temperature reached in our cryogenic setup, 40 mK). With a subsequent increase of the $\text{Cu}_{1-x}\text{Ni}_x$ layer thickness, superconductivity restores again at $d_{\text{CuNi}} \approx 25.5\text{ nm}$, reaching a level of about 0.8 K at $d_{\text{CuNi}} \approx 30\text{ nm}$, and then drops down again below 40 mK at $d_{\text{CuNi}} \approx 37.5\text{ nm}$. This phenomenon of a double suppression of superconductivity is the first experimental evidence for a multiple reentrant behavior of the superconducting state in S/F layered systems.

The data simulation procedure includes coordinated fitting of the $T_c(d_{\text{Nb}})$ and $T_c(d_{\text{CuNi}})$ dependences as shown in Fig. 1.5a, b respectively. The general fitting strategy is described in detail in our previous papers [13, 26]. The solid curves in the figures show results of the calculations for the “clean” case with parameters given in the figure caption. Although we used a common set of parameters at first, the superconducting coherence length, ξ_s , and the magnetic coherence length, ξ_{F0} , were varied within a 5% range, and the S/F interface transparency parameter, T_F , which generally lies in the range $[0, \infty)$, was varied within the range $[0.43, 0.65]$ to obtain better fits for the individual curves. These degrees of freedom that we allowed for the physical parameters are well within the scatter, which can be expected from variations of the deposition conditions from run to run. Calculations with the physical parameters of the S21 sample series, but for a slightly thicker Nb layer $d_{\text{Nb}} \approx 6.3\text{--}6.4\text{ nm}$, show that the next island of superconductivity is possible in the range $d_{\text{CuNi}} \approx 53\text{--}70\text{ nm}$ with maximal T_c of about 0.3 K. We will search for the second reentrance of superconductivity in our further studies.

1.4 Conclusions

To conclude, we report on the experimental observation of the reentrant behavior of superconductivity and a unique double suppression of superconductivity in S/F

bilayers. As S material, Nb with constant layer thickness (≈ 6.2 nm) was used, and as F material $\text{Cu}_{1-x}\text{Ni}_x$ alloy ($x \approx 0.59$) with variable layer thickness. The experimental realization of the reentrant superconductivity phenomenon is an essential progress toward the fabrication of a $F_1/S/F_2$ superconducting spin switch [27–30] for superconducting spintronics.

Acknowledgements The authors are grateful to J. Aarts, C. Attanasio, A.I. Buzdin, M.Yu. Kupriyanov, V. Oboznov, S. Prischepa, and Z. Radovic for stimulating discussions, to J. Lindner, J. Moosburger-Will, and W. Reiber for assistance in TEM sample preparation and measurements. The work was partially supported by DFG through SFB-484, BMBF (project No MDA01/007), RFBR (projects No 07-02-00963, No 08-02-90105-Mol.a, 09-02-12176-ofi.m, 09-02-12260-ofi.m and No 08.820.05.28RF) and the Program of RAS “Spintronics”.

References

1. P.G. De Gennes, E. Guyon, Phys. Lett. **3**, 168–169 (1963)
2. N.R. Werthamer, Phys. Rev. **132**, 2440–2445 (1963)
3. Z. Radović, L. Dobrosavljević-Grujić, A.I. Buzdin, J. Clem, Phys. Rev. B **38**, 2388–2393 (1988)
4. E.A. Demler, G.B. Arnold, M.R. Beasley, Phys. Rev. B **55**, 15174–15182 (1997)
5. A.A. Golubov, M.Yu. Kupriyanov, E. Il’ichev, Rev. Mod. Phys. **76**, 411–469 (2004)
6. I.F. Lyuksyutov, V.L. Pokrovsky, Adv. Phys. **54**, 67–136 (2005)
7. A.I. Buzdin, Rev. Mod. Phys. **77**, 935–976 (2005)
8. F.S. Bergeret, A.F. Volkov, K.B. Efetov, Rev. Mod. Phys. **77**, 1321–1373 (2005)
9. J.S. Jiang, D. Davidović, D.H. Reich, C.L. Chien, Phys. Rev. Lett. **74**, 314–317 (1995)
10. Th. Mühge, N.N. Garif’yanov, Yu.V. Goryunov, G.G. Khaliullin, L.R. Tagirov, K. Westerholt, I.A. Garifullin, H. Zabel, Phys. Rev. Lett. **77**, 1857–1860 (1996)
11. L.V. Mercaldo, C. Attanasio, C. Coccorese, L. Maritato, S.L. Prischepa, M. Salvato, Phys. Rev. B **53**, 14040–14042 (1996)
12. I.A. Garifullin, D.A. Tikhonov, N.N. Garif’yanov, L. Lazar, Yu.V. Goryunov, S.Ya. Khlebnikov, L.R. Tagirov, K. Westerholt, H. Zabel, Phys. Rev. B **66**, 020505 (2002)
13. V.I. Zdravkov, A.S. Sidorenko, G. Obermeier, S. Gsell, M. Schreck, C. Müller, S. Horn, R. Tidecks, L.R. Tagirov, Phys. Rev. Lett. **97**, 057004 (2006)
14. V.V. Ryazanov, V.A. Oboznov, A.Yu. Rusanov, A.V. Veretennikov, A.A. Golubov, J. Aarts, Phys. Rev. Lett. **86**, 2427–2430 (2001)
15. T. Kontos, M. Aprili, J. Lesueur, X. Grisson, Phys. Rev. Lett. **86**, 304–307 (2001)
16. P. Fulde, R. Ferrell, Phys. Rev. **135**, A550–A563 (1964)
17. A.I. Larkin, Yu.N. Ovchinnikov, Zh. Eksp. Teor. Fiz. **47**, 1136–1146 (1964); [Sov. Phys. JETP **20**, 762–769 (1965)]
18. J. Aarts, J.M.E. Geers, E. Brück, A.A. Golubov, R. Coehoorn, Phys. Rev. B **56**, 2779–2787 (1997)
19. L.R. Tagirov, Physica C **307**, 145–163 (1998)
20. M. Born, E. Volf, *Principles of Optics*, 4th edn (Pergamon Press, New York, 1968), Chapter 7
21. T. Tokuyasu, J.A. Sauls, D. Rainer, Phys. Rev. B **38**, 8823–8832 (1988)
22. A. Cottet, W. Belzig, Phys. Rev. B **72**, 180503(R) (2005)
23. A. Cottet, Phys. Rev. B **76**, 224505 (2007)
24. M.G. Khusainov, Yu.N. Proshin, Phys. Rev. B **56**, 14283–14286 (1997); Erratum: Phys. Rev. B **62**, 6832–6833 (2000)
25. B.P. Vodopyanov, L.R. Tagirov, Pis’ma v ZhETF **78**, 1043–1047 (2003); [JETP Lett **78**, 555–559 (2003)]

- 26. A.S. Sidorenko, V.I. Zdravkov, A. Prepelitsa, C. Helbig, Y. Luo, S. Gsell, M. Schreck, S. Klimm, S. Horn, L.R. Tagirov, R. Tidecks, *Ann. Phys.* **12**, 37–50 (2003)
- 27. P.G. De Gennes, *Phys. Lett.* **23**, 10–11 (1966)
- 28. G. Deutscher, F. Meunier, *Phys. Rev. Lett.* **22**, 395–396 (1969)
- 29. L.R. Tagirov, *Phys. Rev. Lett.* **83**, 2058–2061 (1999)
- 30. A.I. Buzdin, A.V. Vedyayev, N.V. Ryzhanova, *Europhys. Lett.* **48**, 686–691 (1999)

Nanoscale Phenomena

Fundamentals and Applications

Hahn, H.; Sidorenko, A.; Tiginyanu, I. (Eds.)

2009, XVIII, 213 p. 139 illus., 33 illus. in color.,

Hardcover

ISBN: 978-3-642-00707-1